

Defect Mediated Desorption of the KBr(001) Surface Induced by Single Highly Charged Ion Impact

R. Heller,* S. Facsko, R. A. Wilhelm, and W. Möller

*Institute of Ion Beam Physics and Materials Research,
Forschungszentrum Dresden-Rossendorf, Bautzner Landstr. 128, 01328 Dresden, Germany*

(Received 16 May 2008; published 26 August 2008)

The individual impacts of slow (300 eV/amu) highly charged Xe ions induce nanometer sized pitlike structures on the KBr (001) surface. The volume of these structures shows a strong dependence on the ions potential energy. Total potential sputter yields from atomically flat (001) terraces are determined by imaging single ion impact sites. The dependence of the sputter yield on the ions initial charge state combined with structure formation at low and high-fluence irradiations indicates that agglomeration of defects into complex centers plays a major role in the desorption process induced by the potential energy.

DOI: [10.1103/PhysRevLett.101.096102](https://doi.org/10.1103/PhysRevLett.101.096102)

PACS numbers: 68.43.-h, 61.72.J-, 61.80.Jh, 79.20.Rf

Slow highly charged ions (HCIs) open specific possibilities of surface structuring due to the dissipation of their potential energy [1]. The high local electronic excitation within the impact site of an HCI is comparable to that induced by swift heavy ion bombardment [2,3] and surface treatment by ultra short laser pulses [4]. However, slow HCI impact is characterized by a much sharper localization of electronic excitation in normal and lateral direction, respectively. Correspondingly, HCIs have been proposed as a tool for surface modifications and analysis on the nanometer scale [5,6]. The potential energy as a unique parameter of HCIs has brought out many new interesting phenomena in ion surface interaction within the last decades as, e.g., hollow atom formation [7], increased secondary electron yields [8], and potential sputtering [9,10]. Furthermore, the potential energy conversion may result in permanent local changes of the electronic structure or changes in the topography of insulating materials [11]. Recently, HCI induced hillock structures have been observed on CaF₂ which have been explained by a solid-liquid phase transition at the surface induced solely by the excitation from the potential energy [12]. For metallic systems the potential energy dissipation was found to contribute less effectively to surface nanostructuring [13].

While energy deposition and sputtering with singly charged ions is mostly well understood, potential sputtering (PS) of insulators by highly charged ions has been much less investigated. Aumayr *et al.* determined total sputter yields of multiply charged Ar and Xe ions on insulating (LiF, NaCl, SiO₂, and MgO), semiconducting (Si and GaAs) and metallic (Au) surfaces by means of a micro balance technique [14]. For insulators, a strongly enhanced sputtering with increasing potential energy was obtained whereas the kinetic energy influences the sputter yield only to a minor extent. The potential sputtering of alkali halides and SiO₂ was explained by desorption mediated by defects created by the electronic excitation [15]. This mechanism had already been identified in the 1970's to be responsible for the electron and ion induced desorp-

tion of alkali halides [16,17]. As a special behavior, the sputtering of MgO shows a pronounced synergism of the potential and the kinetic energy. This so-called kinetically assisted potential sputtering was ascribed to the interaction of kinetically induced lattice distortion with the electronic defects induced by the potential energy dissipation [18]. For semiconductors and metals, no influence of the potential energy on the sputter yields could be identified. The results described above were obtained with polycrystalline samples, and comparatively high ion fluences (10^{13} – 10^{15} cm⁻²) were applied. Thus collective or roughness effects could not be ruled out and local changes of the surface topography associated with potential sputtering could not be observed.

In the present Letter we describe atomic force microscopy studies of KBr(001) single crystals after low-fluence bombardment with multiply charged ($Q = 3, \dots, 34$) slow Xe ions. We show that individual HCI impact leads to the formation of nanometer sized pitlike structures with the depth of one atomic layer. From the atomic force microscopy (AFM) images total sputter yields from atomically flat terraces are determined quantitatively and the morphological changes induced by the potential energy deposition are observed microscopically. Evidence is found that the desorption process is initiated by complex defect centers induced by the high excitation from the potential energy.

KBr single crystals were cleaved in (001) direction in air. Via a transfer system, they were brought into an irradiation chamber with a base pressure of 1×10^{-9} mbar. Subsequently, the samples were heated to a temperature of about 450 K for at least 1 h in order to remove possible contaminants from the surface. During irradiation the samples were kept at room temperature. Highly charged Xe ions ($Q = 3, \dots, 34$) were delivered from an electron beam ion trap (EBIT) [19]. After charge separation via a dipole bending magnet, the ions were decelerated to a fixed kinetic energy of 300 eV/amu by means of a two stage deceleration lens system. A circular ion beam spot of about 2 mm diameter was scanned at

normal incidence over an area of $1\text{ cm} \times 1\text{ cm}$ on the target. After irradiation with fluences from $5 \times 10^9\text{ cm}^{-2}$ to $2 \times 10^{13}\text{ cm}^{-2}$ and fluxes between 1×10^5 and 5×10^8 ions/s which are fairly low enough to prevent any collective effects, the samples were taken out of the vacuum chamber and immediately transferred into the UHV-AFM device (base pressure 1×10^{-10} mbar). The surface topography of the irradiated samples was observed applying contact atomic force microscopy in constant force mode with commercially available silicon cantilevers (tip radius nominally 7 nm) and typically applied forces of 2–3 nN.

Figure 1 shows topographic contact mode AFM images of the virgin surface (a), and after irradiation with Xe^{34+} ions with a potential energy of 23 keV, a kinetic energy of 300 eV/amu, and a fluence of $7 \times 10^9\text{ cm}^{-2}$ (b). Freshly cleaved KBr surfaces typically exhibit large atomically flat terraces of up to $1\text{ }\mu\text{m} \times 1\text{ }\mu\text{m}$ separated by single-step edges, as seen at the upper right edge of frame (a). The irradiated surface features small rectangular pit-like structures with a lateral size of 15–25 nm and a depth of ≈ 0.35 nm, corresponding to one atomic layer. The pit density is in fair agreement with the applied fluence, so we conclude that each HCI creates one pit. The irradiation procedure was repeated on numerous samples for different ion charge states from 3 to 34 to identify the influence of the potential energy on the pit formation.

For each irradiated sample several AFM images were recorded within the beam spot and statistically analyzed with respect to the pit density and volume. Figure 2 shows the measured dependence of the pit volume on the potential energy. The error bars represent the statistical error resulting from the different measurements. The pit volume shows a well-defined linear dependence on the potential energy. Because the pits are only one monolayer deep the volume increase originates from an increased average lateral size (see insets of Fig. 2). The lateral dimensions of the structures are subject to an error by the convolution with the tip shape. With a nominal tip curvature radius of around 7 nm, the error of the volume results as $\approx 10\text{ nm}^3$, which is well within the shown error bars. The minimum resolvable

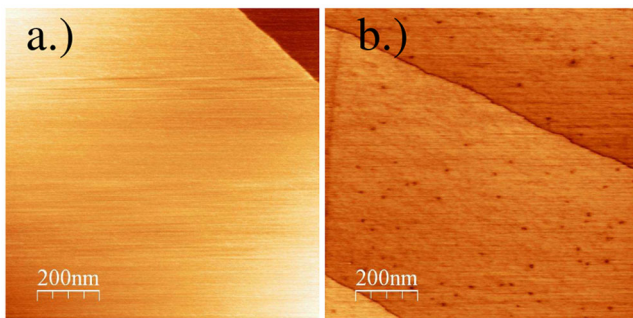


FIG. 1 (color online). Contact mode AFM topographic images of a KBr(001) surface (a) unirradiated, and (b) irradiated with Xe^{34+} at a kinetic energy of 300 eV/amu and a fluence of $7 \times 10^9\text{ cm}^{-2}$. Created nanopits are seen as dark spots in (b).

pit volume is around 10 nm^3 . The right axis in Fig. 2 represents the total sputter yield, which is determined from the pit volume. In the potential energy range of 2–23 keV sputter yields of 800 to 2800 atoms (K + Br) per incident HCI are obtained.

For samples irradiated with lower charge states Q of 3, 5, and 10 no pits could be identified, although the extrapolation of the dashed line in Fig. 2 would predict a size which should be observable within the experimental resolution. Furthermore, one would expect that the extrapolation of the data from Fig. 2 to zero potential energy results in the collisional sputter yield. However, TRIM simulations for Xe ions with a kinetic energy of 300 eV/amu give a sputter yield of only 5 atoms per incident ion, corresponding to a pit volume of $< 1\text{ nm}^3$. This is 2 orders of magnitude below the value expected from the extrapolation, which might indicate that kinetically assisted potential sputtering is also effective in KBr.

It is well known that during electron bombardment of alkali halides monoatomic deep pits are created at the surface by electron stimulated desorption (ESD), which grow and interlink at increasing irradiation time, resulting in a layer by layer erosion [20–22]. A keV electron creates a large number of electron-hole pairs along its trajectory through an ionic crystal. Because of the strong electron-phonon coupling of the ionic lattice these defects become rapidly self-trapped (self-trapped exciton—STE) [21] and subsequently decay into color centers, i.e., an H center (an interstitial molecular halide ion) and an F center (an electron at an anion site). The independent diffusion of both centers and their subsequent recombination with the surface lead to the desorption of halide atoms and alkali atoms, respectively. When the H center recombines with the surface a loosely bound halogen ad-atom is created

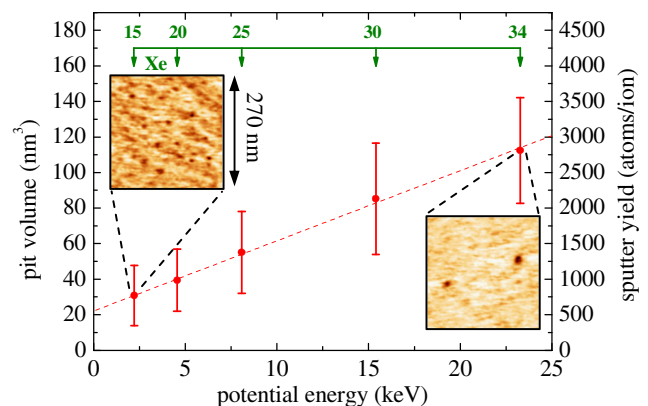


FIG. 2 (color online). Pit volume (left axis) and corresponding total sputter yield (right axis) as a function of the potential energy of the ions. The corresponding charge states are given on the upper scale. The insets show topographic AFM images ($270\text{ nm} \times 270\text{ nm}$) for irradiation with the lowest and highest charge state, at fluences of $3.5 \times 10^{10}\text{ cm}^{-2}$ and $3 \times 10^9\text{ cm}^{-2}$, respectively.

which evaporates thermally. Further, the F center could recombine with the surface by neutralizing an alkali ion leading to its desorption, but as pointed out by Puchin *et al.* [23], an energy deficit exists for this process as long as the F center resides in its ground state. The $2p$ -excited F^* center was found to have enough energy to initiate the alkali atom desorption, and low coordinated surface sites (i.e., terrace edges, kinks, and corners) were found to be preferential points for the desorption process.

Whereas the growth of pits during electron bombardment represents a collective effect requiring several F^* centers to diffuse from the bulk to the surface, the formation of pits by single impact of an HCI, as presented in this work, has to be related to the simultaneous creation of numerous defects within a small area. The interaction between the HCI and the crystal starts from a critical distance r_c (≈ 1 nm) above the surface (see Ref. [24] and references therein). From this point electrons are resonantly captured from the valence band of the surface into highly excited Rydberg states of the approaching ion. A hollow atom (HA) is formed [25]. Subsequent deexcitation of the HA proceeds via nonradiative Auger decay leading to the emission of low energy electrons (≈ 1 eV–100 eV). The electron capture by the incoming ions leaves unbalanced holes within the valence band of the crystal surface. During the impact of the HCI a significant fraction of its potential energy is emitted by energetic (up to keV) inner-shell Auger electrons within the first atomic layers of the crystal on a fs time scale [26]. Further holes are created by resonant neutralization, continuing until the HCI is fully relaxed by Auger decays. These holes can convert into STE by trapping available electrons from the HA decay. Thus a significant number of electronic defects is created within the impact site. In addition high energy Auger electrons from the inner-shell deexcitation can initiate defect creation processes like in the case of ESD. However, the process differs from ESD in two essential points: (i) defect creation takes places in a predamaged surface and (ii) the density of the electrons is much higher than during ordinary electron bombardment.

While the pit growth during ESD can be explained by preferential annihilation of F^* centers at existing step edges, the mechanisms for the creation of the first pits at the very beginning of the desorption process remained so far unclear. Therefore, it was suggested that several F/F^* centers could agglomerate into X centers which should be able to initiate desorption even at the perfect 001 surface [21,27]. However, for ESD it was estimated that the density of F/F^* centers created along the electron trajectory is too low to render this process dominant. In contrast, the HCI impact creates numerous F/F^* centers within a small volume of only a few nm³. In this way, the interaction between defects becomes increasingly important. Since the number of created defects within the volume of interaction depends on the initial charge state (potential energy) of the projectile only, the observed increased volume of the pits

for higher charged states becomes plausible. From the absence of pits for the lowest Xe charge states ($Q = 3, 5,$ and 10) we conclude that a certain number of defects per unit area is necessary to induce this defect agglomeration and thus the desorption.

The defects described above may also be generated by collisional damage along the ion track, which is associated with the kinetic energy of the ion. From TRIM using standard parameters, a total number of roughly 500 collisionally generated Frenkel pairs is obtained which are generated per incident ion within a depth of about 50 nm. Assuming that a significant fraction of these would contribute to desorption via diffusion to the surface, the observed offset in Fig. 2 could be interpreted as an enhancement by kinetic energy deposition, provided the potential energy is sufficient for pit formation.

In order to further elucidate the role of defect agglomeration we performed additional irradiation at higher fluences for two selected charge states $Q = 3$ and $Q = 25$. As shown above, single Xe ion impact for $Q = 3$ does not create any *individual* pits. In contrast, high-fluence irradiation results in the formation of well-defined pits as seen in Fig. 3(a). However, the density of pits is about 3 orders of magnitude less than the applied ion fluence. In accordance with the above considerations, these structures are ascribed to originate from diffusing F^* centers created in the bulk along the ion trajectories (independent on their charge state). This picture is confirmed by the following observations: (i) the pits show a significantly larger spread of their width [see Fig. 3(c)] compared to the pits formed by individual ions of sufficiently high charge state [see Fig. 3(d)], and (ii) within a certain distance to existing terrace edges no pits are found. An F^* center that reaches the surface in the proximity of such a step edge will rather recombine at the low coordinated surface site than create a new pit. Because of the additional desorption from terrace edges for the high-fluence–low-charge state irradiation it is not possible anymore to evaluate sputter yields from the pit volume as described above. Figure 3(b) shows the surface topography after bombardment with Xe²⁵⁺ ions with a fluence of 1×10^{11} cm⁻², which is 100 times higher than in Fig. 1. The corresponding size and depth distribution of pits are shown in Figs. 3(d) and 3(f), respectively. Compared to the low-fluence case, the width distribution broadens by a factor of about two and is only slightly shifted to larger width. However, the depth distribution is now composed of two peaks corresponding to one monolayer and two monolayers, respectively. This is attributed to two subsequent hits of the same surface area. From Fig. 2, the mean pit area at $Q = 25$ is $A = V/0.35$ nm ≈ 150 nm² for single ion impact. For the present fluence $\Phi = 1 \times 10^{11}$ cm⁻² a significant overlap probability $\omega = A \times \Phi = 0.15$ results in rough agreement with the experimental finding [see Fig. 3(f)]. From these measurements we can conclude that the formation of an individual pit by HCI impact is associated with the simultaneous creation and

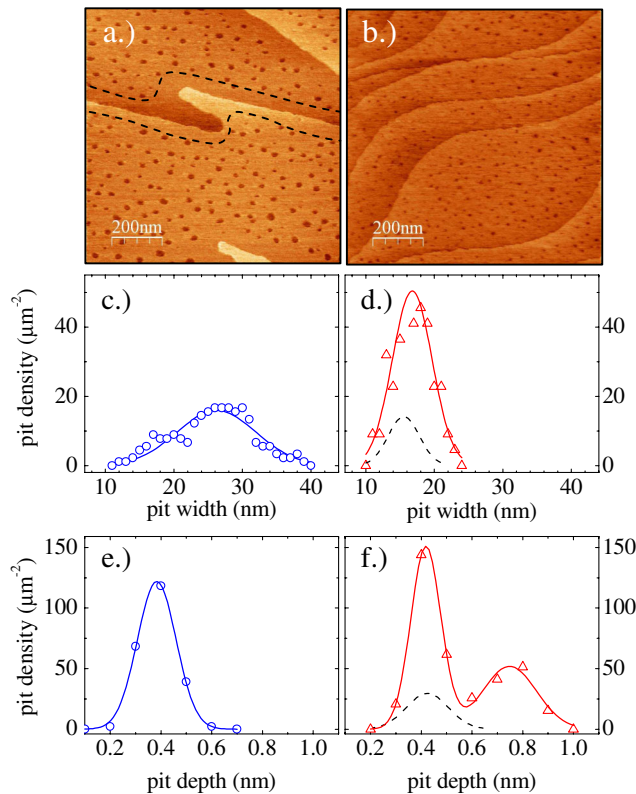


FIG. 3 (color online). Topographic contact AFM images (a), (b) and corresponding distributions of pit width (c), (d) and pit depth (e),(f) for: (a),(c),(e) pits created by collective effects during high-fluence irradiation with Xe^{3+} , $\Phi = 2 \times 10^{13} \text{ cm}^{-2}$, and (b),(d),(f) pits created by single and double impact of Xe^{25+} , $\Phi = 1 \times 10^{11} \text{ cm}^{-2}$. The fluence in (b),(d), (f) is 200 times smaller than in (a),(c),(e) but also 10 times higher than for the single impact irradiation like shown in Fig. 1. The dashed lines in (c),(f) show the corresponding size distribution from a low-fluence ($\Phi < 1 \times 10^{10} \text{ cm}^{-2}$) irradiation.

agglomeration of numerous Frenkel defects within a certain area, in clear contrast to diffusion driven pit creation induced by high-fluence irradiation at low charge state.

In summary, single impact of highly charged Xe ions was found to initiate the formation of pit structures on KBr (001) with lateral sizes of 10–25 nm and monoatomic depth. The mean pit volume and thereby the total sputter yield depend linearly on the potential energy of the ions. The pit formation is ascribed to a desorption mediated by defects, which are generated by the release of the potential energy of the ions close to the surface and by collisional damage along the ion track. The creation of individual pits by each projectile and complementary high-fluence irradiations with low charge state offer evidence for the formation of F center agglomerates (X centers) on the KBr surface within the impact sites.

This work was financially supported by the European project ITS LEIF (No. RII3/026015) JRA6. We thank N. Stolterfoht and Z. Pesic for helpful discussion and

valuable comments on the manuscript.

*r.heller@fzd.de

www.fzd.de

- [1] D. Kost, S. Facsko, W. Möller, R. Hellhammer, and N. Stolterfoht, *Phys. Rev. Lett.* **98**, 225503 (2007).
- [2] F. Thibaudau, J. Cousty, E. Balanzat, and S. Bouffard, *Phys. Rev. Lett.* **67**, 1582 (1991).
- [3] E. Akcoltekin, T. Peters, R. Meyer, A. Duvenbeck, M. Klusmann, I. Monnet, H. Lebius, and M. Schleberger, *Nature Nanotech.* **2**, 290 (2007).
- [4] A. C. Tien, S. Backus, H. Kapteyn, M. Murnane, and G. Mourou, *Phys. Rev. Lett.* **82**, 3883 (1999).
- [5] F. Aumayr and H. P. Winter, *e-J. Surf. Sci. Nanotech.* **1**, 171 (2003).
- [6] F. Schenkel *et al.*, *Phys. Scr.* **T80A**, 73 (1999).
- [7] A. Arnau *et al.*, *Surf. Sci. Rep.* **27**, 113 (1997).
- [8] H. Kurz, K. Toglhofer, H. P. Winter, F. Aumayr, and R. Mann, *Phys. Rev. Lett.* **69**, 1140 (1992).
- [9] T. Schenkel *et al.*, *Nucl. Instrum. Methods Phys. Res., Sect. B* **161**, 65 (2000).
- [10] F. Aumayr, P. Varga, and H. P. Winter, *Int. J. Mass Spectrom.* **192**, 415 (1999).
- [11] I. C. Gebeshuber, S. Cernusca, F. Aumayr, and H. P. Winter, *Int. J. Mass Spectrom.* **229**, 27 (2003).
- [12] A. S. El-Said *et al.*, *Nucl. Instrum. Methods Phys. Res., Sect. B* **258**, 167 (2007).
- [13] J. M. Pomeroy, A. C. Perrella, H. Grube, and J. D. Gillaspay, *Phys. Rev. B* **75**, 241409(R) (2007).
- [14] F. Aumayr and H. Winter, *Phil. Trans. R. Soc. London* **362**, 77 (2004).
- [15] M. Sporn, G. Libiseller, T. Neidhart, M. Schmid, F. Aumayr, H. P. Winter, P. Varga, M. Grether, D. Niemann, and N. Stolterfoht, *Phys. Rev. Lett.* **79**, 945 (1997).
- [16] D. J. Elliott and P. D. Townsend, *Philos. Mag.* **23**, 249 (1971).
- [17] J. P. Biersack and E. Santner, *Nucl. Instrum. Methods* **132**, 229 (1976).
- [18] G. Hayderer *et al.*, *Phys. Rev. Lett.* **86**, 3530 (2001).
- [19] G. Zschornack, F. Grossmann, R. Heller, M. Kreller, U. Kentsch, S. Landgraf, and Ovsyannikov, *Nucl. Instrum. Methods Phys. Res., Sect. B* **256**, 565 (2007).
- [20] B. Such, P. Czuba, P. Piatkowski, and M. Szymonski, *Surf. Sci.* **451**, 203 (2000).
- [21] B. Such, J. Kolodziej, P. Czuba, P. Piatkowski, P. Struski, F. Krok, and M. Szymonski, *Phys. Rev. Lett.* **85**, 2621 (2000).
- [22] H. Hoche, J. P. Toennies, and R. Vollmer, *Phys. Rev. Lett.* **71**, 1208 (1993).
- [23] V. Puchin, A. Shluger, Y. Nakai, and N. Itoh, *Phys. Rev. B* **49**, 11364 (1994).
- [24] L. Hagg, C. O. Reinhold, and J. Burgdörfer, *Phys. Rev. A* **55**, 2097 (1997).
- [25] J. Burgdörfer, P. Lerner, and F. W. Meyer, *Phys. Rev. A* **44**, 5674 (1991).
- [26] H. Winter and F. Aumayr, *J. Phys. B* **32**, R39 (1999).
- [27] J. J. Kolodziej *et al.*, *Surf. Sci.* **482**, 903 (2001).